

Full Wave Analysis of Passive Microwave Monolithic Integrated Circuit Devices Using a Generalized Finite Difference Time Domain (GFDTD) Algorithm.

Faiza S. Lansing
California Institute of Technology
Jet Propulsion Laboratory
Pasadena, California

Daniel L. Rascoe
California Institute of Technology
Jet Propulsion Laboratory
Pasadena, California

ABSTRACT

This paper presents a modified Finite-Difference Time-Domain (FDTD) technique using a generalized conformed orthogonal grid. The use of the Conformed Orthogonal Grid, Finite Difference Time Domain (GFDTD) enables the designer to match all the circuit dimensions, hence eliminating a major source of error in the analysis. The method proves to be a powerful and efficient tool for modeling complicated microstrip circuits. From LHC time domain results, the frequency-dependent parameters of a millimeter-wave branch line coupler, a dual-stub filter, and a 3-dimensional package are computed. Accuracy verification of the model is further achieved by comparing the results with those obtained from measurements, when available, and other commercial software tools.

INTRODUCTION

Developing low-cost, compact, densely packed, and high-performance Monolithic Microwave Integrated Circuits (MMIC's) is a major technology thrust. To reduce the time and cost of the hardware iterative design cycle, and to increase the probability of first pass designs, rigorous analysis tools are needed to provide reliable predictions of the performance parameters.

Simple discontinuities, such as bends, tee- and cross-junctions, step in widths, etc., are basic components of any complex microstrip circuits [1 - 4]. To model such circuits, designers usually use the quasi-static analysis that is based on empirical low-frequency formulae. However, this quasi-static analysis does not accurately evaluate the characteristics of monolithic circuits at microwave or millimeter-wave frequencies since it does not account for radiation, coupling, fringing, and wave propagation effects. Some circuits, such as patch antennas, radial stubs, or spur filters, cannot be investigated using the quasi-static analysis because of the high radiation, and coupling effects. In such a case, more rigorous techniques, that provide an exact, or full-wave, solutions of Maxwell's equations are needed. One of the analysis tools, that is straight forward, versatile, and has acquired many new applications, is the Finite-Difference Time-Domain (FDTD), however the FDTD does not allow the designer to match all circuit dimensions. A new generalized 3-D conformed orthogonal grid, Finite Difference Time Domain (GFDTD) technique, presented in this paper, matches all circuit dimensions, and compensates for the deficiency in the FDTD technique. The GFDTD is designed to handle predominantly planar multilayered microstrip structures. Interlayer transitions such as striplines and vias can be easily simulated. The GFDTD proves to be flexible in handling a variety of complex circuit configurations.

Three sample structures are selected from a variety of test cases to demonstrate the versatility of the GFDTD technique and for the verification of the model. Three structures are modeled. A millimeter-wave branch line coupler fabricated on gallium arsenide (GaAs) substrate with $\epsilon_r = 12.9$; a dual-stub low-pass filter fabricated on an Alumina substrate with $\epsilon_r = 9.9$, and a 3-Dimensional package fabricated on a Alumina substrate with $\epsilon_r = 9.9$. All the circuits represent resonant microstrip structures fabricated on an open substrate: hence, radiation and coupling effects dominate the performance significantly. The results of using the conformed orthogonal grid technique to the analysis of frequency-dependent scattering parameters and the performance of complex geometry printed microstrip circuits are presented. The GFDTD scattering parameters are further compared with the available measurements and computed results from a commercial software (nodal simulator) for the fabricated circuits.

GOVERNING EQUATIONS

The GFDTD method begins by considering the partial differential form of the two Maxwell's curl equations that govern the propagation of electric and magnetic fields in structures.

$$\mu \frac{\partial \vec{H}}{\partial t} = -\nabla \times \vec{E} \quad (1)$$

$$\epsilon \frac{\partial \vec{E}}{\partial t} = \nabla \times \vec{H} - \sigma \vec{E} \quad (2)$$

Where μ is permeability of the medium in hmu-y/meter, ϵ is the permittivity of the medium in farad/meter, σ is conductivity of the medium in sicmens/meter, E is electric field intensity in volt/meter, H is the magnetic field intensity in ampere/meter, and t is the time elapsed in seconds. To find an approximate solution to equations (1) and (2), the finite difference method is commonly used to discretize the three dimensional space and time domains and add the appropriate boundary conditions.

A. Finite-Difference Equations

In 1966, Yee [1] has developed a technique to solve the two Maxwell's curl equations. The six field components ($E_x, E_y, E_z, H_x, H_y, H_z$) are considered to be interleaved in space and are placed as shown in the elemental cell of Figure 1. The entire space domain no matter how complex it can be, is obtained by stacking these parallelepiped cells into a larger 3-D configuration. The $x, y,$ and z dimension of the elemental cell are $\Delta x, \Delta y,$ and $\Delta z,$ respectively.

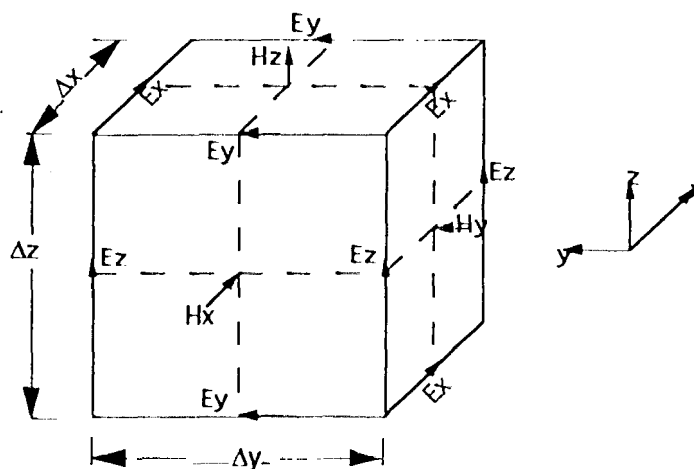


Figure 1. Field components placed in an FDTD elemental Cell (uniform grid)

Using the above arrangement notation for the E and H fields, the explicit finite difference forms of equations (1) and (2) for $E(\vec{r}, t)$ and $H(\vec{r}, t)$ are found [3],

B. Model Adaptation for Conformed Grids

The use of uniform grids, in most cases, contribute to errors [2]. To avoid such errors we adapted Yee's finite difference equations to suit conformed grids, producing the GFDTD technique, which offer a superior solution by avoiding errors resulting in mismatching the actual boundaries of the structure. As shown in Figure 2, electric field components (E white dots with black arrows, H in black dots) take new values at the boundaries between two consecutive non uniform spacing.

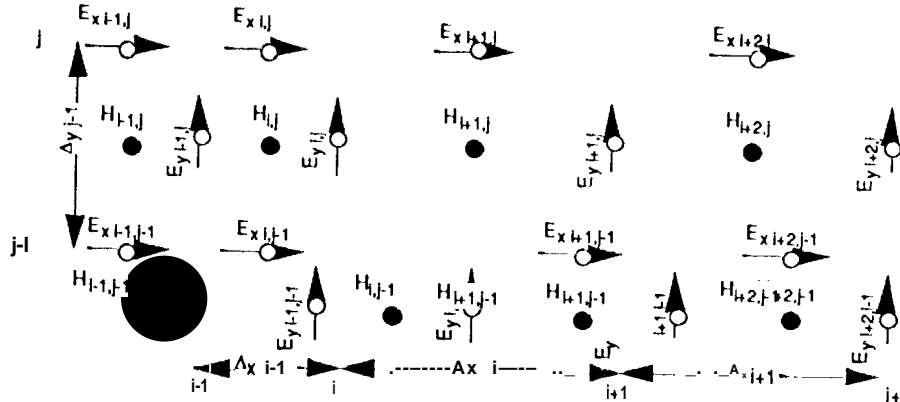


Figure 2. Field components in the x-y plane for a conformed grid

Hence, for conformed grids the finite difference equations for H_x , H_y , H_z remain unchanged while equations are:

$$H_{xi,j,k}^{n+\frac{1}{2}} = H_{xi,j,k}^{n-\frac{1}{2}} + \frac{\Delta t}{\mu \Delta z} (E_{yi,j,k}^n - E_{yi,j,k-1}^n) - \frac{\Delta t}{\mu \Delta y} (E_{zi,j,k}^n - E_{zi,j-1,k}^n) \quad (3)$$

$$H_{yi,j,k}^{n+\frac{1}{2}} = H_{yi,j,k}^{n-\frac{1}{2}} + \frac{\Delta t}{\mu \Delta x} (E_{zi,j,k}^n - E_{zi-1,j,k}^n) - \frac{\Delta t}{\mu \Delta z} (E_{xi,j,k}^n - E_{xi,j,k-1}^n) \quad (4)$$

$$H_{zi,j,k}^{n+\frac{1}{2}} = H_{zi,j,k}^{n-\frac{1}{2}} + \frac{\Delta t}{\mu \Delta y} (E_{xi,j,k}^n - E_{xi,j-1,k}^n) - \frac{\Delta t}{\mu \Delta x} (E_{yi,j,k}^n - E_{yi-1,j,k}^n) \quad (5)$$

$$E_{xi,j,k}^{n+1} = \left[\frac{1 - \frac{\sigma \Delta t}{2\epsilon}}{1 + \frac{\sigma \Delta t}{2\epsilon}} \right] E_{xi,j,k}^n + \frac{1}{1 + \frac{\sigma \Delta t}{2\epsilon}} \left\{ \frac{2\Delta t}{\epsilon(\Delta y_{j+1} + \Delta y_j)} \left[H_{xi,j+1,k}^{n+\frac{1}{2}} - H_{xi,j,k}^{n+\frac{1}{2}} \right] - \frac{2\Delta t}{\epsilon(\Delta z_{k+1} + \Delta z_k)} \left[H_{yi,j,k+1}^{n+\frac{1}{2}} - H_{yi,j,k}^{n+\frac{1}{2}} \right] \right\} \quad (6)$$

$$E_{yi,j,k}^{n+1} = \left[\frac{1 - \frac{\sigma \Delta t}{2\epsilon}}{1 + \frac{\sigma \Delta t}{2\epsilon}} \right] E_{yi,j,k}^n + \frac{1}{1 + \frac{\sigma \Delta t}{2\epsilon}} \left\{ \frac{2\Delta t}{\epsilon(\Delta z_{k+1} + \Delta z_k)} \left[H_{xi,j+1,k}^{n+\frac{1}{2}} - H_{xi,j,k}^{n+\frac{1}{2}} \right] - \frac{2\Delta t}{\epsilon(\Delta x_{i+1} + \Delta x_i)} \left[H_{zi+1,j,k}^{n+\frac{1}{2}} - H_{zi,j,k}^{n+\frac{1}{2}} \right] \right\} \quad (7)$$

$$E_{zi,j,k}^{n+1} = \left[\frac{1 - \frac{\sigma \Delta t}{2\epsilon}}{1 + \frac{\sigma \Delta t}{2\epsilon}} \right] E_{zi,j,k}^n + \frac{1}{1 + \frac{\sigma \Delta t}{2\epsilon}} \left\{ \frac{2\Delta t}{\epsilon(\Delta x_{i+1} + \Delta x_i)} \left[H_{yi+1,j,k}^{n+\frac{1}{2}} - H_{yi,j,k}^{n+\frac{1}{2}} \right] - \frac{2\Delta t}{\epsilon(\Delta y_{j+1} + \Delta y_j)} \left[H_{xi,j+1,k}^{n+\frac{1}{2}} - H_{xi,j,k}^{n+\frac{1}{2}} \right] \right\} \quad (8)$$

The GFDTD forward difference approximation is used to calculate the spatial partial derivatives instead of the centered difference used in equations [1-4]. The forward difference technique is first-order accurate, which may cause slight errors, when integrating for a large number of time steps. With this fact in mind, the GFDTD is only applied to determine the E fields at the boundaries of two consecutive layers of different spatial size, while Yee's equations [1] are used to compute the E fields within each layer. Also, the reader should be aware that the changes in spatial increment between layers is restricted to $\pm 30\%$. Better accuracy can be achieved if an interpolation technique is used, such as a splint to determine the spatial partial derivative of the magnetic field exactly at the interface between the two different layers.

C. Selection of size of Time Step

For the conformed grid, the size of the time step is based on modifying the stability criteria [2] to take into consideration the changing spatial steps. For l number of Δx 's, m number of Δy 's, and n number of Δz 's, the size of time step in a conformed grid computation, is determined from:

$$\Delta t \leq \min \left[\frac{1}{v_{\max}} \left(\frac{1}{\Delta x_i^2} + \frac{1}{\Delta y_j^2} + \frac{1}{\Delta z_k^2} \right)^{-\frac{1}{2}} \right] \quad (9)$$

Where $i=1, 2, \dots, l$; $j=1, 2, \dots, m$; $k=1, 2, \dots, n$ and Δt is chosen as the minimum of the permutation generated by varying i, j, k .

Equations (3) through (9) give an approximate solution of $E(\vec{r}, t)$ and $H(\vec{r}, t)$ in the computational domain (or grid). Special considerations are required, however, for the source and the mesh walls, as discussed in section D.

D. Treatment of the Source, and Absorbing Boundary Conditions

1. Source Considerations

A Gaussian-shaped pulse is chosen as the source excitation at time $t=0$. This choice is advantageous because its frequency spectrum is also Gaussian. By adjusting the width of the pulse, the spectrum provides frequency-domain information ranging from dc to the desired cutoff frequency.

$$E_z = f_z(t) = e^{-\frac{(t-t_0)^2}{\tau^2}} \quad (10)$$

The Gaussian-shaped pulse excitation will result in the fundamental mode propagating down the microstrip in the frequency range of interest.

2. Absorbing Boundary Conditions

One of the six mesh boundaries is a ground plane and its tangential electric field values are set to be zero everywhere on the plane. The tangential electric field components on the remaining five mesh boundaries must be specified such that outgoing waves are not reflected, i.e., absorbed. Mur's [5] second-order approximate absorbing boundary condition is used to enforce the above non-reflection constraints, as shown below:

$$\begin{aligned} \Phi_0^{n+1}(i, k) = & -\Phi_1^n(i, k) + \frac{c\Delta t - \Delta y}{c\Delta t + \Delta y} \Phi_0^n(i, k) + \frac{2\Delta y}{c\Delta t + \Delta y} \Phi_1^n(i, k) \\ & + \frac{(c\Delta t)^2 \Delta y}{2\Delta x^2 (c\Delta t + \Delta y)} \left[\Phi_0^n(i+1, k) - \Phi_0^n(i, k) + \Phi_0^n(i-1, k) + \Phi_1^n(i+1, k) - \Phi_1^n(i, k) + \Phi_1^n(i-1, k) \right] \\ & + \frac{(c\Delta t)^2 \Delta y}{2\Delta z^2 (c\Delta t + \Delta y)} \left[\Phi_0^n(i, k+1) - \Phi_0^n(i, k) + \Phi_0^n(i, k-1) + \Phi_1^n(i, k+1) - \Phi_1^n(i, k) + \Phi_1^n(i, k-1) \right] \end{aligned} \quad (11)$$

Where c is the speed of light in vacuum, Φ is the desired parameter to be absorbed at the boundaries. Note that this expression is valid only for the x - z plane. Similar expressions can be derived for x - y and y - z planes.

E. Calculation of Frequency-Dependent Parameters

In addition to the time domain results (E, H , voltages, and currents), obtained by the GFDTD method, the frequency-dependent scattering parameters, characteristic impedance, and effective dielectric constant, which augment the analysis are calculated.

The scattering parameters provide a measure for the circuit performance. To calculate scattering parameters, the total vertical electric field underneath the center of each microstrip port is recorded at every time step and integrated along the z -direction as shown in figure 3-a. To obtain the scattering parameter $S_{11}(o)$, the incident and reflected voltage must be determined by calculating the incident and reflected voltages at the input port (port 1). The incident voltage, V_{inc} is determined by assuming an infinite microstrip line, which extends from

source to the far absorbing wall. The same process is repeated using the actual microstrip structure, yielding the total voltage, V_{1t} at the input port. The reflected voltage, V_{1ref} is determined by subtracting the incident voltage from the total voltage at the input port. At the other ports only transient waveforms will be computed. The scattering parameters, S_{11} , S_{21} , and S_{12} are then obtained by simple Fourier transform of the voltages. The current $I(t)$ is computed at the port by integrating the magnetic field over the contour C as shown in Figure 3-b.

The characteristic impedance, $Z_0(\omega)$ of a microstrip line is defined at the fundamental mode of propagation, as the ratio of the voltage to the current in the frequency domain.

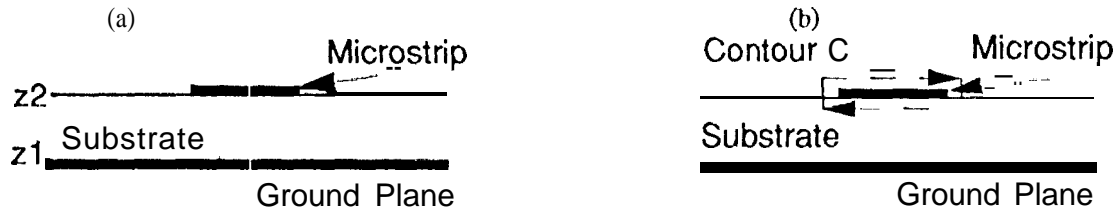


Figure 3 Configuration for computing the total voltage and current at the ports

RESULTS

The three structures used in testing the GFDTD model with conformed grid arc as follows: a branch line coupler; a dual stub filter; and a 3-dimensional package. The first circuit is fabricated on gallium arsenide (GaAs) substrate with $\epsilon = 12.9$ and a thickness of $100 \mu\text{m}$. The dual stub filter is constructed on Alumina substrate with $\epsilon = 9.9$ and a thickness of 0.005 inch (0.127 mm), and a 3-dimensional package fabricated on an Alumina substrate with $\epsilon = 9.9$ and a thickness of 0.3 millimeters . The three circuits have dimensions of less than 1 cm , and the frequency range of interest is from dc to 50 GHz . Although the operating frequency of all circuits is less than 50 GHz ; the GFDTD is able to provide an insight to the performance of these circuits outside the operating range. Scattering matrix coefficients are measured for the dual stub filter, the using an HP 8510 network analyzer, which is calibrated between 2 to 45 GHz . Measurements for the millimeter-wave branch line coupler and the 3-D package are not available.

A. Millimeter-wave Branch Line Coupler

The selected branch line coupler, is shown in Figure 4, divides power equally between ports 2 and 4 from either ports 1 or 3. This occurs at the center frequency, where the center-to-center distance between the four lines is a quarter wavelength ($\lambda/4$). Also, at the center frequency, the phase difference between ports 2 and 4 is 90° . The total number of grid points is $49 \times 100 \times 16$. The thickness of the substrate is modeled as $3 \Delta z$, while the air space above is modeled as $13 \Delta z$.

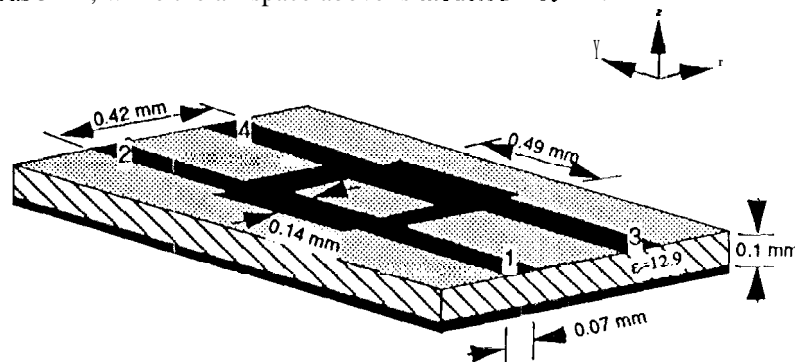


Figure 4. Millimeter-wave branch line coupler detail,

The center to center distance are $14 \Delta x$ and $14 \Delta y$. The distance from the source plane to the edge of the coupler is $40 \Delta y$, and the reference planes for ports 1 through 4 are $10 \Delta y$ from the edges of the coupler. The strip widths of ports 1 through 4 are modeled as $2 \Delta x$. The wide strips in the coupler are modeled as $4 \Delta x$ wide.

The time step Δt is 0.05 ps. The Gaussian half-width, T is 5 ps and the time delay, t_0 , is set to $3T$. The simulation is performed for 4000 time steps to allow the response on all four ports to reach zero. The computation time using the CRAY Y-MPW116 is less than 2 minutes for the conformed grid.

The scattering coefficient results, are shown in Figure 5. The desired branch line coupler performance is witnessed in the sharp S_{11} and S_{13} nulls which recur at approximately the same point (49 GHz) as the crossover in S_{12} , and S_{14} . At this crossover point S_{12} and S_{14} are both about -3 dB, indicating that the power is being evenly divided between ports 2 and 4. The nulls in S_{11} and S_{13} at the operating frequency indicate that little power is being transmitted by ports 2 and 4. The phase difference between S_{12} and S_{14} , is verified to be approximately 90° at the operating point (≈ 49 GHz). This behavior is also predicted by Compact Explorer software.

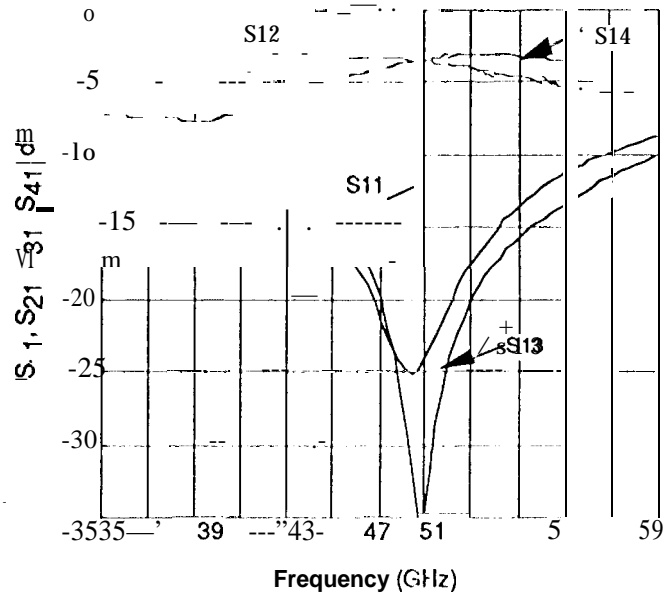


Figure 5 Scattering parameters for the millimeter-wave branch line coupler

B. Microstrip Dual-Stub filter

The dual stub filter analyzed is based on the design used by Texas Instrument and the University of Colorado, MI MICAD Center [6]. The dimensions are shown in Figure 6. The total number of grid points representing this filter is $120 \times 68 \times 16$. The operating resonance (≈ 10 GHz) corresponds to the frequency where $L = \lambda/4$, and $S = \lambda/16$ and the distance between the center of each stub and the ports is $k/32$. For the GFDTD, $2 \Delta x$, $2 \Delta y$, and one Δz are carefully chosen to fit the dimensions of the circuit. The long rectangular patch is thus $2 \Delta x$'s by $68 \Delta y$'s. Each stub is modeled as $46 \Delta x$ by $2 \Delta y$. The thickness of the substrate is selected as $2 \Delta z$, the remaining $14 \Delta z$ represent the air space above the substrate.

$L = 2.921$ mm
 $S = 0.75692$ mm
 $a = 0.44196$ mm

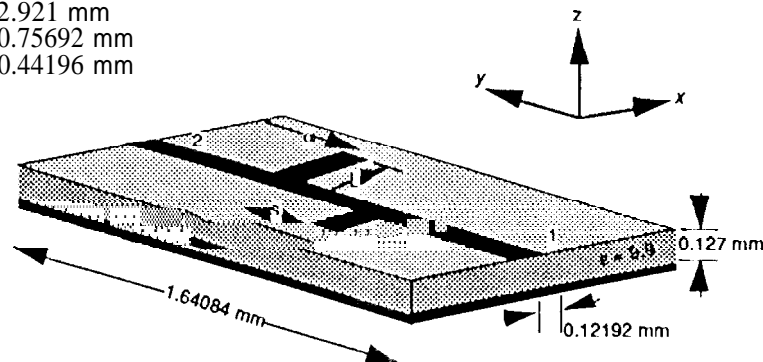


Figure 6 Double-stub filter detail

The time step, Δt used is 0.117 ps. The Gaussian half-width is $T = 10$ ps and the time delay t_0 is set to be $3T$. The simulation is performed for 15000 time steps to allow the response at both ports to become 0. Due to the circuit higher dielectric constant, the phase speed is lower and more samples, i.e., time steps, are needed to fully simulate the behavior of the circuit. The computation time for this circuit is approximately 18 minutes on the CRAY-MPW116 compared to 2 hours per each frequency for an HP workstation [6].

The resulting scattering coefficient $|S_{21}|$ is plotted in Figure 7-a for GFDTD, superimposed on the measured data. Good agreement is evident at the location of the response nulls. The desired low-pass filter performance is witnessed by the steep S_{21} roll-off beginning at approximately 8 GHz. The narrowing in the stopband determined from the GFDTD model, may be due to the approximation of using the forward difference technique for the conformed grid. In comparing the scattering parameters determined from measurements with the results determined from the nodal simulator, shown in figure 7-b it is obvious that the nodal simulator, lacks the capability to predict the performance of this filter. Additionally the nodal simulator is unable to predict the dual response nulls as expected from having dual stubs but is predicts correctly the location of one resonating frequency qualitatively and overestimates the depth of the response nulls.

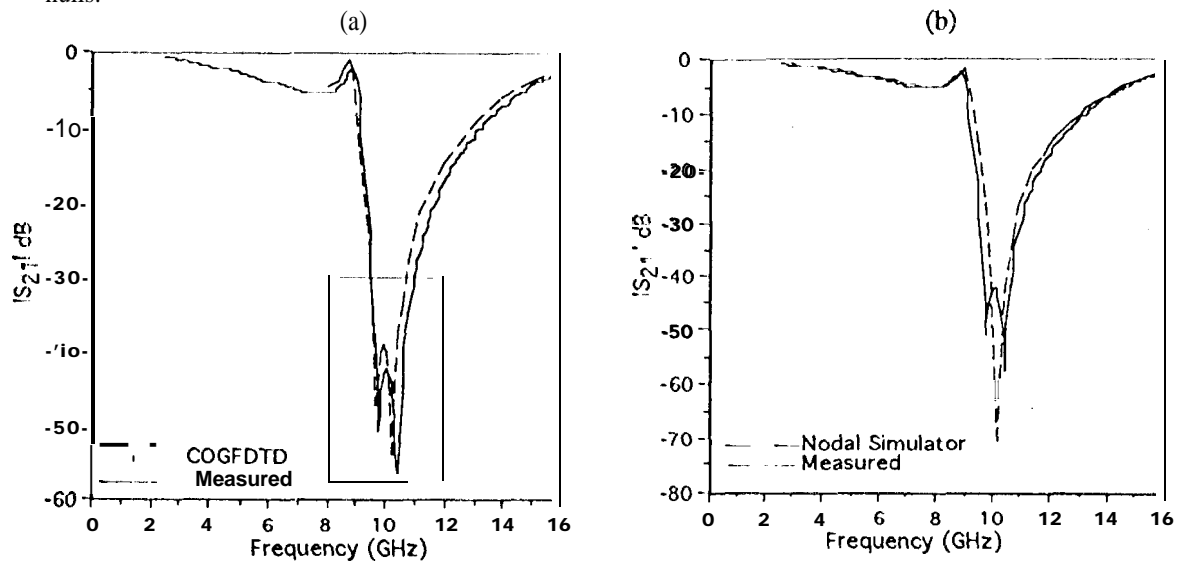


Figure 7 Insertion loss of a dual stub filter

C. 3-Dimensional Package

The 3-Dimensional Package is designed and fabricated on an Alumina substrate with $\epsilon = 9.9$. The 3-D package dimensions are shown in Figure 8. The space steps Δx , Δy , and Δz are chosen to match all circuit dimensions. The iris circuit is the most complicated, in all the cases treated in this paper, because it has multilayers. The total physical dimension of this package is 9 mm x 4.02 mm x 3 mm, which transferred 67x 150x61 grid points. The thickness of the substrate is modeled as $10 \Delta z$ while the air spaces above and below the substrate are modeled as $25 \Delta z$ each.

The design procedure presented in [7] have been followed carefully for this circuit to yield the desired performance parameters.

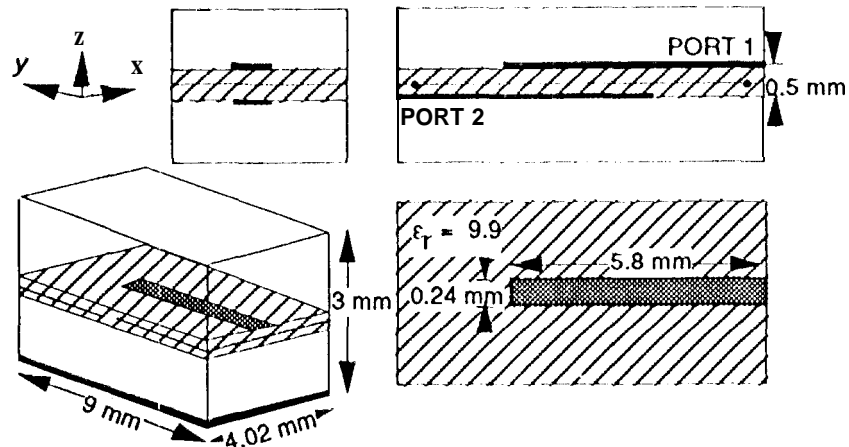


Figure 8. Detail of 3-Dimensional Package

The time step Δt is 0.1 ps. The Gaussian half-width, T is 15 ps and the time delay, t_0 , is set to $3T$. The simulation is performed for the GFDTD for 3000 time steps to allow the response on the two ports to reach zero. The computation time using the CRAY Y-MP2E/116, is less than 10 CPU minutes

The frequency response presented in figure 9, demonstrates the utility of this structure as an interconnect. The desired frequency response, i.e., center frequency, bandwidth, and shape is obtained by the proper selection of geometry. As shown in figure. 9, the insertion loss at the center frequency is less than 0.2 dB and a very wide bandwidth is achievable, which makes this design versatile specially at higher frequencies.

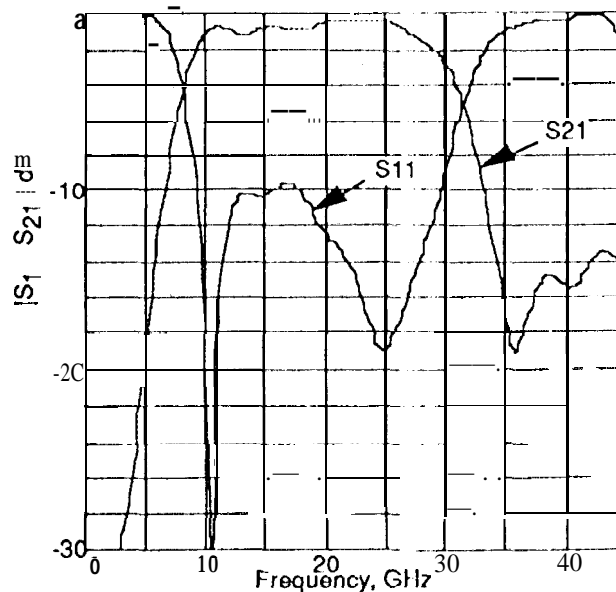


Figure 9. Scattering parameters for the 3-Dimensional Package

CONCLUSIONS

For the conformed orthogonal grid, the Generalized finite-difference time-domain method, GFDTD, has been used to perform time-domain simulations of pulse propagation in three printed microstrip circuits. Frequency-dependent scattering parameters, and characteristic impedance, have been calculated by Fourier transform of the time-domain results. The results are validated either by comparison with the results obtained from measured data taken from fabricated circuits, or results obtained from the nodal simulator. The versatility of the GFDTD method allows easy and accurate calculation of many complicated microstrip structures. It should be noted that simpler models, such as nodal simulator, are still highly useful for "first cut designs" of microstrip circuits since they allow

for **quick** solution and, in some cases, allow for **intuition** about devices being modeled. The **GFDTD** method can then be applied to determine the performance of the actual circuit more accurately.

The versatility of the **GFDTD** method **allows** for matching all circuit dimensions and for direct calculation of performance parameters for many complicated **microstrip** structures. The structures analyzed in this paper were selected so **that** comparisons **could** be made with other publications or measurements or **methods** of analysis. With the computational power of **supercomputers** increasing rapidly, such as the **CRAY Y-MP2E/16**, time savings in the order of 200 to 1 is **achieved** compared to the VAX workstation. The **fast**, accurate, **GFDTD** now lends itself as a computer aided design of many complex geometries of **microstrip** circuit components.

A video tape that **visualizes** the electric and magnetic fields as they **evolve** in time was produced.

ACKNOWLEDGMENT

This research was carried **out** in part by the Jet Propulsion Laboratory, California **Institute** of Technology, under a **grant** with the National Aeronautics and Space Administration. This research was also performed in part using the Jet Propulsion Laboratory/California Institute of technology **CRAY Y-MP2E/16 Supercomputer**. Access to this facility **was** provided by the Jet propulsion Laboratory Supercomputing project.

REFERENCES

- [1] K. S. Yee, "Numerical solution of initial **boundary** value problems in isotropic media," *IEEE Transactions on Antennas and Propagation*, vol. AP-14, pp. 302-307, May 1966.
- [2] D. Sheen, S. Ali, M. **Abouzahra** and J. A. Kong, "Application of the three-dimensional **finite-difference time-domain** method to the analysis of planar **microstrip** circuits," *IEEE Transactions on Microwave Theory and Techniques*, vol. 38, pp. 849-856, July 1990.
- [3] X. **Zhang**, J. Fang, K. **Mei** and Y. Lui, "Calculations of the dispersive characteristics of **microstrips** by the time-domain **finite difference** method," *IEEE Transactions on Microwave Theory and Techniques*, vol. 36, pp. 263-267, July 1988.
- [4] X. **Zhang** and K. **Mei**, "Time-domain **finite difference** approach to the calculation of the frequency-dependent **characteristics** of **microstrip discontinuities**," *IEEE Transactions on Microwave Theory and Techniques*, vol. 36, pp. 1775-1787, July 1988.
- [5] D. M. **Sheen**, "Numerical Modeling of **Microstrip** Circuits and Antennas". Ph.D. dissertation, **Massachusetts Institute** of Technology, June 1991.
- [6] Private communication with Dr. Doris Wu, **MMICAD** Center, University of Colorado, Boulder, Mars 1992,
- [7] Vandenberg, N. L., "Full-Wave Analysis of **Microstrip-Fed** Antennas and Couplers", Ph.D. dissertation, The University of Michigan, 1991.